Two-Way Coupled Large-Eddy Simulations of the Gas-Solid Flow in Cyclone Separators

J. J. Derksen and H. E. A. van den Akker
Multi-Scale Physics Dept., Delft University of Technology, Prins Bernhardlaan 6, 2628 BW Delft, Netherlands

S. Sundaresan
Dept. of Chemical Engineering, Princeton University, Princeton, NJ 08544

DOI 10.1002/aic.11418
Published online February 28, 2008 in Wiley InterScience (www.interscience.wiley.com).

Three-dimensional (3-D), time-dependent Eulerian-Lagrangian simulations of the turbulent gas-solid flow in cyclone separators have been performed. The gas flow is simulated with the lattice-Boltzmann method. It solves the filtered Navier-Stokes equations, where the Smagorinsky subgrid-scale model has been used to represent the effect of the filtered scales. Through this large-eddy representation of the gas flow, solid particles with different sizes are tracked. By viewing the individual particles (of which there are some 10^7 inside the cyclone at any moment in time) as clusters of particles (parcels), the effect of particle-to-gas coupling on the gas-flow and particle behavior at modest mass-loadings (up to 0.2 kg dust per kg air) is studied. The numerical approach is able to capture the effect of mass loading on the swirl intensity as reported in the experimental literature. The performance of a Stairmand high-efficiency cyclone under various loading conditions is systematically studied. The presence of solid particles causes the cyclone to lose swirl intensity. Furthermore, the turbulence of the gas flow gets strongly damped. These two effects have significant consequences for the performance of the cyclone. The pressure drop monotonically decreases with mass loading. The collection efficiency responds in a more complicated manner to the mass loading, with mostly increased cut sizes, and increased overall efficiencies.
 AIChE J, 54: 872–885, 2008
Keywords: computational fluid dynamics (CFD), multiphase flow, particle technology, separation techniques

Introduction

Cyclone separators are widely used devices for separating components with different densities contained in process streams. The driving force for separation is the centrifugal force which is induced by bringing the stream in a strongly swirling motion. Examples are oil-water separation in oil production, removal of liquid droplets from gas streams (demisting), and cleaning gas streams contaminated with solid particles (dedusting). Specifically the latter application has important environmental implications; industrial dust emission regulations are getting stricter as high-concentrations of fine dust particles in the atmosphere form a serious threat to human health. Cyclones are energy efficient and low-maintenance separation devices; they contribute in a very economical manner to dust emission reduction and air quality improvement. Improved cyclone design, specifically toward reducing the cut size could enhance the role of cyclones in industrial cleaning further.

Whereas from an operational point of view gas cyclones are very simple devices, their fluid dynamics and related particle motion is complex. Process streams are usually such

Correspondence concerning this article should be addressed to J. Derksen at jos@ualberta.ca.

that the flow is turbulent. This turbulent flow has a strong swirl component which has very pronounced impact on the flow characteristics, including the structure of the turbulent fluctuations.[1–3] Swirling flows often behave in a counterintuitive manner showing phenomena like vortex breakdown, vortex core precession and a strong sensitivity to the downstream flow conditions. Turbulence gets strongly anisotropic under strong swirling conditions and sometimes the flow partly laminarizes.[4] This picture gets even more complicated if we introduce particles. Not only are the particles centrifuged out due to the swirling motion, they also feel the turbulent motion of the gas that tends to disperse them throughout the cyclone. In fact, the grade efficiency curve (the relation between separation efficiency and particle size for specific cyclone geometry and operation conditions) reflects the competition between centrifugal force that drives particles to the outer wall of the cyclone, and turbulence that disperses the particle throughout the entire volume, the strength of both effects being a pronounced function of the particle size. Contrary to some models for predicting cyclone efficiency and cut size,[5,6] we hardly see a role for the average (inward) radial velocity in the separation process. From validated numerical simulations[7] it has become apparent that the levels of the fluctuating gas velocity are much higher than the average radial velocity in virtually every part of the cyclone.

To further complicate the picture, there is clear experimental evidence[8,9] that the performance of gas cyclones is influenced by the solids mass loading. At loadings in the range from zero to roughly 10^{-1} kg dust per kg air the overall efficiency improves significantly. The pressure drop reduces with increased mass loading. This teaches us that particle-particle, or particle-to-gas coupling (or both) are relevant for the separation process. Based on their experimental findings, Hoffmann et al.[8] speculate that the reason for the mass loading effects is that in the inlet region bigger particles sweep smaller particles with them toward the wall, that is, a mechanism related to particle-particle interaction. We think, however, that appreciable effects of particle-particle collisions are not very likely for the situations at hand with solids volume fractions of the order of 10^{-5}. Muschelknautz[10] introduced the concept of critical loading and developed an analytical model to account for the efficiency improvement. In this model, the efficiency improves monotonically with increasing mass loading. While this has been a very successful model for quantifying the experimental data at low-mass loading levels, it does not give a direct explanation as to how such a loading effect comes about through underlying physical processes.

In a previous article,[11] we speculated that gas-particle interaction was responsible for the mass loading effects. This was based on preliminary results of numerical simulations. It was argued that the particles have a twofold effect on the gas-flow in the cyclone: they reduce the swirl intensity, thereby deteriorating the separation process,[12,13] and they reduce the turbulence intensity, thereby improving separation. The former effect explains why the pressure drop reduces with increased mass loading: reduced swirl implies less wall friction. The latter effect (turbulence damping by small particles) has been extensively reported in the experimental and computational literature.[14,15] It is not *a priori* clear, however, what the net effect on the separation process would be as a result of swirl reduction *and* turbulence reduction occurring at the same time. This we investigate further in this article, again by means of numerical simulation. We will show that the swirl reduction by particles occurs in a monotonic and rather uniform manner. The turbulence reduction by the particles varies less systematically, leading to a more complicated response of the cyclone in terms of its collection efficiency. The purpose of this article is to reveal the interactions between various physical mechanisms that eventually determine the performance of cyclones. It is not our goal to present a numerical method for cyclone simulation to be used for (day-to-day) design purposes. For such purposes the computational demands (run times and memory resources) are impractically large.

In a series of articles,[4,7,11,16] we have developed a numerical procedure based on large-eddy simulation (LES) to accurately represent confined, turbulent, swirling flow. Flow field results showed very good agreement with experimental data both in terms of the average, as well as the fluctuating velocities (the latter being at least as important as the former in relation to dust separation). In the flow field we subsequently introduce particles of various sizes that we track. Based on the fate (collected or exhausted) of the particles with various sizes, grade efficiency curves can be constructed.

Obermair et al.[17] directly measured the effects of solids on (swirl) velocity profiles in the lower parts of a cyclone separator. We have simulated their experimental configuration in order to further validate our numerical procedure, specifically the representation of the effects the particles have on the gas-flow. The main focus of this article, however, is on the Stairmand high-efficiency cyclone. For this cyclone we systematically simulated the effect of mass loading on cyclone performance, and checked the effects of specific modeling assumptions, among other things the particle-wall interaction.

This article is organized in the following manner. We start with a brief recapitulation of the essentials of the numerical procedure, and of the modeling assumptions we make. We then discuss the cases studied experimentally by Obermair et al.[17,18] that we use for validation purposes. In the main part of the article we introduce and then describe the results of the Stairmand cyclone simulations. The article closes with a summary of the main findings.

Numerical setup

The 3-D, time-dependent, incompressible Navier-Stokes equations that govern the motion of the continuous gas-phase were discretized by means of the lattice-Boltzmann method.[19,20] This method was chosen for its geometrical flexibility in combination with numerical efficiency (especially on parallel computer platforms). The method uses a uniform, 3-D grid consisting of cubic cells. Therefore, a single parameter (the lattice spacing Δ, expressed as a fraction of the main cyclone dia. D) fully defines the spatial resolution of a simulation. In the cubic grid, curved walls can be accurately and efficiently implemented by means of a forcing (or immersed boundary) method.[21–23] Since generally the Reynolds numbers in gas-cyclones are too high for full resolution of all details of the turbulent gas flow we need turbulence modeling. In our recent articles, we have shown that for

swirling flows a large-eddy simulation (LES) approach to turbulence modeling is feasible and leads to accurate predictions. In LES the larger, inherently 3-D and time-dependent turbulent flow structures are explicitly resolved, whereas the smaller eddies and the impact they have on the bigger scales are modeled. The distinction between resolved and unresolved length scales is made by the computational grid. The impact of the unresolved (subgrid-scale) motion on the resolved (grid-scale) motion has been modeled with the standard Smagorinsky subgrid-scale model[24] with Smagorinsky constant $c_S = 0.1$. This model views the subgrid-scale motion as diffusive with an eddy-diffusivity proportional to the local (resolved) deformation rate. In order to force unresolved fluctuation levels to zero in the vicinity of no-slip walls, wall functions were applied.

The outflow boundaries of strongly swirling flow require special care since swirl can induce subcritical behavior.[25] Subcriticality implies that disturbances do not only propagate downstream, but also upstream. As a consequence, there potentially is a strong dependency of the flow field on the outflow boundary conditions. As we did in previous simulations[7]—inspired by Benjamin's work[26]—the flow at the exit boundary was forced to a critical state by placing a small disk closely upstream of the outflow boundary. At the actual outflow boundary a zero velocity gradient condition was applied. We checked and found no significant dependence of the size or the exact placement of the disk on the results.

The 3-D procedure for simulating unsteady swirling flow as applied in this research and sketched above was able to represent cyclonic flow,[7] and the flow in a through-flow swirl tube[4] very well. Vortex breakdown closely downstream contractions in through-flow devices were predicted in agreement with flow visualization experiments due to Escudier et al.[25] Vortex core precession frequencies in a Stairmand cyclone as measured[27] and simulated agreed to within 10%. A comparison of measured and simulated velocity profiles (averaged velocities and RMS values, the latter quantifying the turbulence intensity) yielded very good results.

The Reynolds number that fully defines the gas flow was defined as $Re = \frac{U_{in}D}{\nu}$, where D is the (main) diameter of the cyclone, U_{in} the superficial inlet velocity, and ν the kinematic viscosity of the continuous phase fluid (air under atmospheric conditions).

Solid, spherical particles (dia. d_p) were introduced in the gas stream. Their location $\mathbf{x_p}$ was updated according to $\frac{d\mathbf{x_p}}{dt} = \mathbf{v_p}$; the evolution of the particle velocity $\mathbf{v_p}$ obeyed Newton's second law with the particle feeling Stokes drag and gravity

$$\frac{d\mathbf{v_p}}{dt} = \frac{U_{in}}{Stk\,D}\left(\mathbf{u} - \mathbf{v_p}\right) + \mathbf{g} \tag{1}$$

with $\mathbf{u}$ the gas velocity at the location of the particle, and $\mathbf{g}$ the gravitational acceleration vector, and Stk the Stokes number (defined as $Stk = \frac{\rho_p}{\rho_g}\frac{d_p^2 U_{in}}{18\nu D}$). Stokes drag is a fair approximation for the conditions considered here. Particle sizes are of the order of a few microns, slip velocities of the order of a few meters per second at most, and air under atmospheric conditions is the working fluid. This means particle Reynolds numbers not exceeding unity, and Stokes drag being 15% off at most (according to the Schiller and Naumann[28] drag relation).

The Stokes number is here defined as the ratio of the particle relaxation time, and the gas-flow integral time scale $T_{int} = \frac{D}{U_{in}}$. In LES, the gas velocity $\mathbf{u}$ in Eq. 1 is composed of a resolved part and a subgrid-scale part representing the unresolved gas velocity. The former was determined by linear interpolation of the velocity field at the grid nodes to the particle position, the latter is mimicked by a Gaussian, isotropic stochastic process with zero average and an RMS value $u_{sgs} = \sqrt{\frac{2}{3}k_{sgs}}$. The SGS kinetic energy k_{sgs} can be estimated from the SGS model and the assumption of local equilibrium.[29] We earlier demonstrated[7] for one-way coupled simulations that for sufficiently fine grids the SGS motion of the gas was such that it hardly had any influence on the motion of the solid particles. We, therefore, conclude that our LES resolves most of the scales relevant for the dynamics of the particles, even the ones significantly smaller than the cut size of the cyclone. This is a great advantage of LES over solving the Reynolds averaged Navier-Stokes (RANS) equations. If particles are released in a RANS gas-flow field, the dispersion due to turbulence needs to be stochastically modeled, which is quite a speculative exercise, especially in relation to mimicking the spatial and temporal coherence in a turbulent flow.

In the simulations, we achieve two-way coupling by feeding back the force that the gas exerts on the particles as a source term to the filtered Navier-Stokes equations. Even when we consider only modest particle mass loading levels (of say, 0.01), the total number of particles inside the cyclone becomes extremely large, and tracking the motion of all these particles is computationally unaffordable. Therefore, we track only a representative set of particles and postulate that each simulated particle represents a large number of identical particles (present at the same location as the tracked particle). In other words, we view the individual numerical particles as parcels, i.e., as assemblies of particles. In this way, we limit the number of tracked particles to a few million. We then multiply the gas-to-particle force by the number of particles in the parcel before we feed it back to the gas-phase.

The drag force (being the only hydrodynamic force considered here) multiplied by the number of particles in a parcel γ is linearly distributed over the eight lattice nodes surrounding the particle (particle source in cell (PSIC) approach, Crowe et al.[30]). To avoid strong force fluctuations that would destabilize the numerical scheme we under-relax the particle-to-fluid force

$$\mathbf{F}_{ijk}^{n+1} = \left(1-\alpha\right)\mathbf{F}_{ijk}^{n} - \alpha\gamma\sum_{m}\beta_{m,ijk}^{n+1}\mathbf{F}_{D,m}^{n+1} \tag{2}$$

with $\mathbf{F}_{ijk}^{n}$. the particle-to fluid force at lattice site i,j,k at time instant n, and $\mathbf{F}_{D,m}^{n}$ the drag force acting on the particle (and, thus, $-\mathbf{F}_{D,m}^{n}$ the force acting on the gas) with index m (in the vicinity of i,j,k), where again the upper index n indicates the time-step number. The weight factor $\beta_{m,ijk}^{n}$ of the drag force distribution over the neighboring lattice site ijk depends on the particle position relative to the lattice, and, therefore, depends on time. The relaxation factor α was set to 0.03. The time constant of the under-relaxation process is then of

the order of 30 (time steps). Particles generally travel much less than half a lattice spacing in 30 time steps.

In the simulations, the particles did not interact with one another, i.e., a particle does not undergo collisions with other particles (and, therefore, particles are allowed to overlap). Based on the space averaged solids volume fraction that is of the order of 10^{-5} this is a fair assumption. However, since the bigger particles accumulate at the outer wall, locally the solids volume fraction becomes one to two orders of magnitude higher, and we enter a region where particle-particle collisions may become important. However, we do not expect these near wall regions to significantly alter the turbulence.

In the simulations, the default settings for particle-wall collisions are such that collisions are elastic and frictionless (smooth walls). We have checked the impact of these assumptions by performing a simulation with rough walls that we mimic with diffusive reflections of particles, and a restitution coefficient of 0.9.

Obermair et al.[17,18] cyclone

For a number of reasons, the way we perform particle-to-gas coupling is a critical (and to some extent speculative) part of our numerical approach. In the first place we use the concept of parcels; in the second place we have noncolliding particles; in the third place we let the particle-to-gas forces only act on the resolved velocity field (i.e., the back coupling forces are only incorporated in the filtered Navier-Stokes equations), not on the SGS gas motion. The latter point implies that we assume the particles do not directly modulate the turbulence at the subgrid scales.

In order to check if the particle-to-gas coupling as implemented in our modeling strategy does predict qualitatively and quantitatively the right trends, we turned to the experimental work due to Obermair and coworkers.[17,18] Their experiments are very important for a number of reasons, specifically since they provide experimental gas swirl profiles with and without dust particles.

The specific geometry that has been investigated is given in Figure 1. Gas-flow patterns in various geometries as measured with laser Doppler anemometry (LDA) were presented in Obermair et al.[18] The emphasis in the experiments was on the lower parts of the cyclones, including the dust bin. Our main interest was in their geometry C, as in a subsequent article[17] in this geometry swirl profiles in the presence of dust were presented. Results of the gas-only flow large-eddy simulations at $Re = 3.4 \cdot 10^5$ (based on $D = 0.4$ m as defined in Figure 1, and $U_{in} = 12.7$ m/s corresponding to an air flow rate of 800 m^3/h), including comparison with LDA results are presented in Figure 2. In this figure, we have selected three representative axial levels in the cyclone. From bottom to top: in the dustbin, in the downcomer, and in the conical part. Average velocities and RMS levels of the fluctuating velocity in axial and tangential direction are shown. The LES was performed with two spatial resolutions corresponding to a lattice spacing of $\Delta = D/144$, and $\Delta = D/200$. Both spatial resolutions imply large grids. The total number of cells being $2.5 \cdot 10^7$ and $6.7 \cdot 10^7$, respectively. The (parallel) efficiency of the lattice-Boltzmann method allows for running such large simulations on relatively low-end parallel platforms (PC-clusters). For completing typically 20 integral time scales (D/U_{in}), gas-only simulations run for a few (5 to 10) days on typically 10 CPU's in parallel. If we add particles to the cyclones, run times increase dramatically. Not so much because of the computational load needed for handling particle transport (this load is comparable to the gas-flow part of the code), but because it may take some hundred integral time scales before the particle concentration field settles in a quasi-steady state.

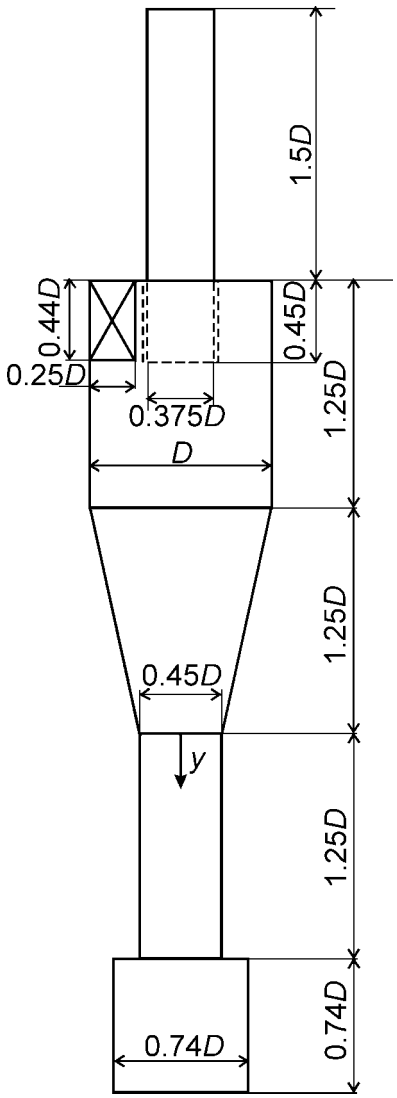

Figure 1. Cyclone geometry due to Obermair et al.[18]

The definition of the y-coordinate is the same as in the cited article. $D = 400$ mm.

As can be concluded from the results presented in Figure 2, we need the fine spatial resolution to accurately predict the average flow in the lower part of the cyclone. Especially to represent the complicated shape of the profiles of the axial velocity requires big grids. The tangential velocity profiles are less sensitive to the resolution. The predictions of the velocity fluctuation levels are of comparable quality as the average velocity. As explained earlier, a good representation of the turbulence is essential for realistic predictions of particle motion in cyclones. The convergence is in the right direction:

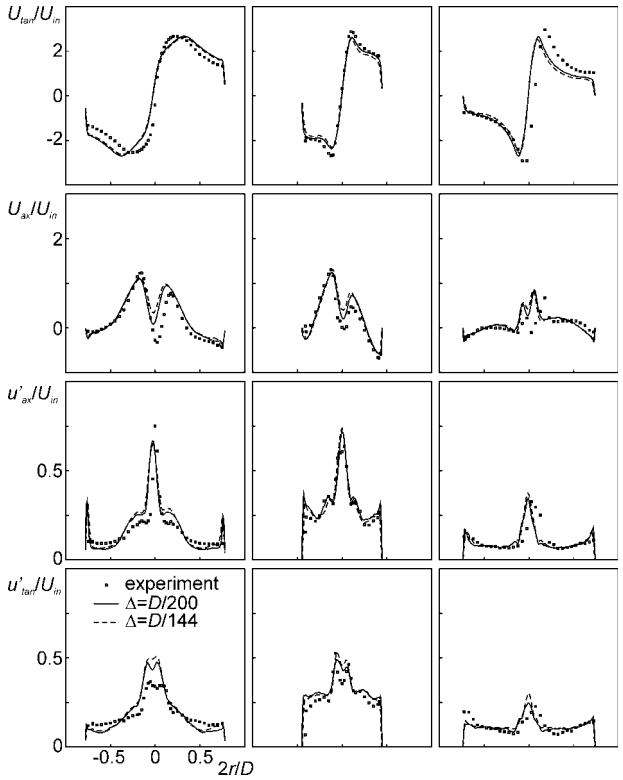

Figure 2. Radial profiles of the tangential and axial velocity at three axial levels in the Obermair et al.[17,18] cyclone at $Re = 3.4 \cdot 10^5$.

Comparison of experimental data,[18] and single-phase LES on two grids. From top to bottom: average tangential velocity, average axial velocity, RMS of axial velocity, RMS of tangential velocity. From left to right: $y = -0.75D$, $y = 75D$, $y = 1.625D$.

the finer the grid, the better the agreement with the experimental data. To see how the swirl profiles change as a result of the presence of dust, we introduce solid particles in the flow. Starting with a fully developed single-phase flow field, we introduce 2.3 kg of dust consisting of uniformly sized particles with $d_p = 5.4$ μm (solids density $2.8 \cdot 10^3$ kg/m^3, $Stk = 8.1 \cdot 10^{-4}$) in the lower part of the cyclone ($y > 0$). The solids mass is distributed over 10^7 parcels, with 1 parcel representing 10^6 solid particles. These particles are bigger than the cut-size of the cyclone under the current operation conditions ("coarse dust"); therefore, most of them stay in the lower part of the cyclone. Only once in a while a particle exits through the vortex finder at the top. This allows us to collect steady-state statistics of the gas velocity in the presence of particles. For reasons of computational demand, we could not do these two-phase simulations on the fine ($\Delta = D/200$) grid; we had to revert to the coarser grid with $\Delta = D/144$.

The loading condition in the two-phase simulation has been chosen such that it corresponds more or less to the experimental conditions of Figure 8 of the article by Obermair et al.[17,31] The total amount of "coarse dust" in the experiment was approximately 2.5 kg, its mean particle size was around 5 μm. The size distribution was skewed toward bigger particles: 5% of the mass was contained in particles bigger than 13 μm; also 5% of the mass was contained in particles smaller than 2 μm. Obermair et al.'s[17,18] gas velocity profiles in the presence of particles zoom in on the flow in the downcomer: it considers four radial profiles of tangential velocity at axial levels in the range $y/D = 0.1$ to 1.02. In Figure 3 we have reproduced the experimental data from Obermair et al.[17] (and scaled them with U_{in} and D) and plotted them along with our simulation data.

The effect of the dust on the gas velocity is very pronounced. The experiments reveal two effects: a broadening of the vortex core, and a reduction of the tangential velocity. The deeper in the downcomer, the larger the differences between single and two-phase flow, eventually in the lower part of the downcomer the swirl profile has transformed from a Rankine type vortex to a relatively weak solid-body rotation. The simulations show the same trends, but to a different extent. The broadening of the vortex core is less than in the experiment; the swirl reduction is bigger up in the downcomer, and weaker deep in the downcomer. Given the width of the particles-size distribution in the experiment vs. the uniform particle size in the simulation, we cannot expect close agreement between the measured and simulated two-phase flow fields.

Figure 4 shows the time-averaged particle transport in the downcomer and dustbin. It confirms the qualitative picture as sketched in Obermair et al.,[17] and shows the significant transport of particles between the various parts of the cyclone. On the bottom of the cyclone, near the center, particles are entrained by the gas flow and circulate in its lower part. The level of asymmetry in Figure 4 is of a comparable level as

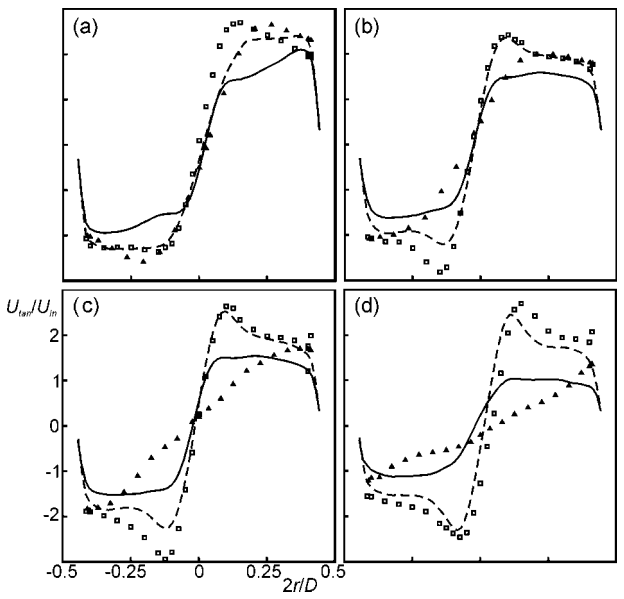

Figure 3. Radial profiles of the tangential gas velocity for various axial positions (chosen according to the experimental data in Figure 8 of Obermair et al.[17]) in the downcomer.

Panel (a): $y/D = 0.1$, (b): $y/D = 0.575$, (c): $y/D = 0.695$, (d): $y/D = 1.02$. Symbols are experimental data[17] for single phase (squares), and two-phase (triangles) flow. Curves are our LES with resolution $\Delta = D/144$. Dashed curve: single-phase flow; solid curve: two-phase flow.

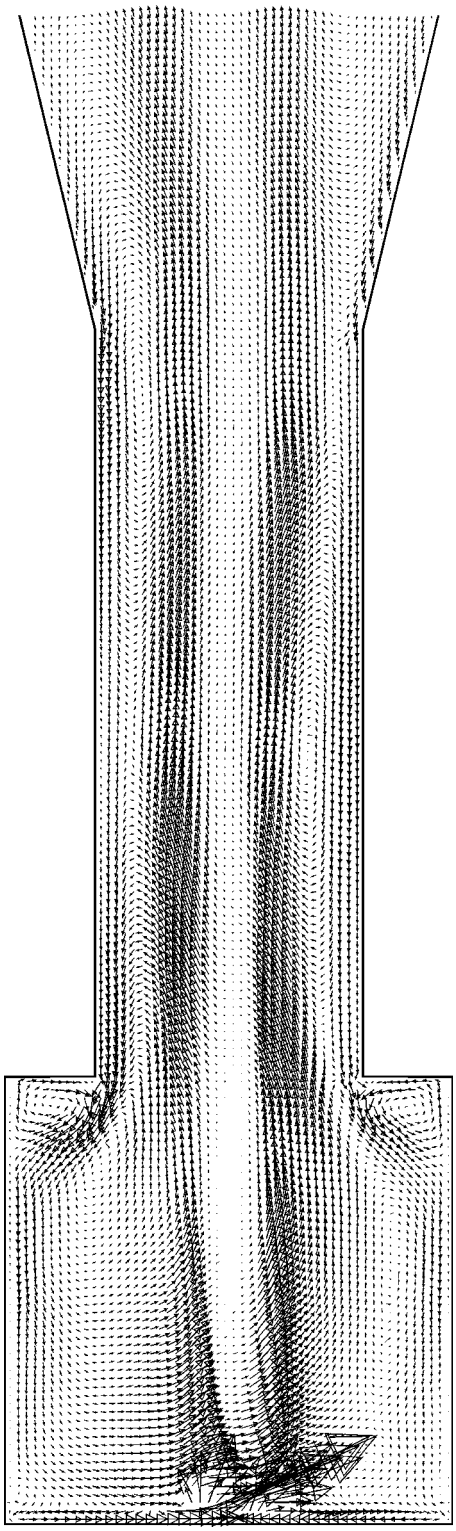

Figure 4. Particle flux vectors (local particle velocity times particle concentration) in the lower part of the Obermair et al.[17,18] cyclone for a two-way coupled, two-phase simulation with particles of 5.4 μm.

the asymmetry observed in the experiments by Obermair et al.[17,18] It is induced by the asymmetric placement of the inlet channel.

Based on the comparison with Obermair et al.'s[17,18] experiments, we conclude that our representation of the way the particles couple back to the gas flow leads to a fairly realistic modulation of the flow in the cyclone. We now turn to the Stairmand cyclone and systematically investigate the impact the flow modulation has on the separation process.

Stairmand High-Efficiency Cyclone

Setup of the simulations

The Stairmand cyclone geometry we have used in this article (see Figure 5) is the same as the one used by Derksen[7], and Derksen et al.[11] The former article only considered

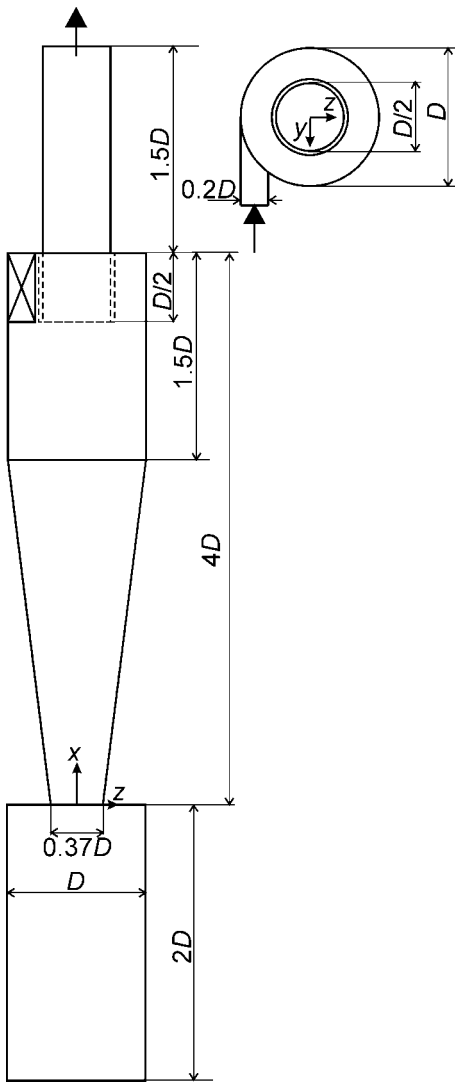

Figure 5. Flow geometry and coordinate system of the Stairmand cyclone: left: side view, right: top view.

single-phase and one-way coupled two-phase simulations. The quality of the single-phase flow predictions was assessed extensively against experimental data, and was comparable to the quality of the single-phase results we obtained with the Obermair et al.[17,18] cyclone as presented in Figure 2. All Stairmand simulations were done with the same Reynolds number: $Re = 2.8 \cdot 10^5$ (with the Reynolds number based on the main body dia. D as defined in Figure 5). The particles that were fed to the cyclone had a uniform size distribution (in terms of numbers of particles) with nine different, logarithmically spaced Stokes numbers ($Stk = 3.0 \cdot 10^{-4}$, $5.0 \cdot 10^{-4}$, $8.3 \cdot 10^{-4}$, $1.4 \cdot 10^{-3}$, $2.3 \cdot 10^{-3}$, $3.9 \cdot 10^{-3}$, $6.5 \cdot 10^{-3}$, $1.1 \cdot 10^{-2}$, $1.8 \cdot 10^{-2}$). These values were chosen to lie around the cut-size $Stk_{50} = 1.5 \cdot 10^{-3}$, as it was determined from previous one-way coupled simulations.[7] The gravitational acceleration was such that the Froude number amounted to $Fr = \frac{U_{in}^2}{D|\mathbf{g}|} = 90$. The major variable in the simulations presented here was the mass loading. An overview of the Stairmand cases we studied is given in Table 1. Please note that by definition the simulations with mass loading $\phi_m = 0.0$ are one-way coupled (particles feeling the gas, the gas not feeling the particles), and the cases with $\phi_m < 0$ are two-way coupled.

To get an idea of physical dimensions: the laboratory-scale Stairmand cyclone Hoekstra[27] used for his gas flow and separation experiments (the latter were used by Derksen[7] for validation purposes), had a diameter of $D = 90$ cm, and a typical inlet velocity of 16 m/s. If we consider calcium carbonate as the particulate material ($\rho_p = 2740$ kg/m^3), the range of particle sizes we consider is between 1.4 and 11 μm.

Since we want to investigate turbulence modification due to particles, we need to let the system evolve to a representative, quasi-steady distribution of the solids phase throughout the cyclone. In order to initialize such a distribution, and to have a reference case, we first initialized the one-way coupled simulation (Case 1, see Table 1). This case was started with a fully developed flow and a cyclone without any particles. Subsequently, particles were continuously fed into the cyclone at a rate of $1.24 \cdot 10^5$ particles per T_{int}. They were randomly distributed over the inlet area and had a uniform particle-size distribution (i.e., the nine Stokes numbers were equally represented numberwise). In order to reach a steady state, particles not only need to be exhausted through the exit pipe at the top, but also need to be extracted at or closely above the bottom of the dustbin. Particles are considered exhausted (i.e., caught in the exit stream at the top) once they cross the $x/D = 5.5$ plane (see Figure 5 for a definition of the coordinate system attached to the Stairmand cyclone). It was assumed that once a particle was below $x/D = -1.9$, i.e., $0.1D$ above the bottom of the dustbin, it could be considered collected by the cyclone (i.e., we assume the chance of such a particle to re-entrain small), and was no longer taking part in the simulation. The $x/D = -1.9$ position is to some extent arbitrary. It is a compromise between putting it very closely above -2.0 which turns out to be computationally expensive (many particles getting almost stuck in the boundary layer at the bottom), and putting it higher up which is physically not realistic (not enough particles in the dustbin to alter the flow once we switch on the two-way coupling). The boundary condition for the gas flow remains unchanged at the bottom: at $x/D = -2$ there is a no-slip wall.

Table 1. Stairmand Cyclone Simulation Cases

Case #	Solids Mass Loading ϕm	# Particles/ Parcel γ	Wall-Collisions*	Remarks
1	0.0	n.a.	sesr	
2	0.0	n.a.	dre0.9	wall-collision sensitivity
3	0.00156	$1.23 \cdot 10^4$	sesr	
4	0.00625	$4.94 \cdot 10^4$	sesr	
5	0.0125	$9.88 \cdot 10^4$	sesr	
6	0.025	$1.98 \cdot 10^5$	sesr	
7	0.05	$3.95 \cdot 10^5$	sesr	
8	0.1	$7.90 \cdot 10^5$	sesr	
9	0.1	$1.58 \cdot 10^6$	sesr	γ senstivity
10	0.2	$1.58 \cdot 10^6$	sesr	

*sesr = smooth, elastic specular reflection; dre0.9 = diffuse reflection, $e = 0.9$.

In order to determine collection efficiencies as a function of the Stokes number, the two-phase flow system has to get to a steady state first. This can be checked by considering the particle fluxes through the inlet, the exhaust at the top, and the bottom. In Figure 6 we show quasi-steady state time series of particle fluxes at three Stokes numbers for the zero mass loading case. Especially the fluctuations in time of the fluxes of the bigger particles through the bottom are considerable. They have a time-scale of the order of $30T_{int}$. For a statistically sound estimate of (steady-state) grade efficiencies, we need to run the simulation for typically four to five times that time (120–$150T_{int}$) after quasi-steady state has been reached.

The way a two-way coupled simulation reaches the steady state is shown in Figure 7 (for the case with mass loading 0.025). This simulation was started from a one-way coupled (mass loading zero) simulation. At $t = 0$, the particle-to-gas coupling was switched on. The gas-solid flow responds very strongly to this: it exhausts large amounts of particles through the bottom. Apparently the two-way coupled gas flow in the dustbin was not capable anymore of carrying the large amounts of particles that were there in the one-way coupled case. The time period for transiting to the new steady state belonging to $\phi_m = 0.025$ is approximately $100T_{int}$ (see Figure 7). The rest of the time series ($t = 100$ to $220\ T_{int}$) has been used for determining the steady-state collection efficiency.

Spatial-solids distribution in the cyclone

The snapshots (taken at a moment after steady state was reached) of the particle distribution in a cross section through the center of the cyclone as given in Figure 8, allow for a few important qualitative observations. It should first be noted that in Figure 8 we are actually looking at parcels, in the sense that the dots are parcels each representing a number of particles. The number of parcels in the cyclone, and especially in the lower part of the cyclone decreases with increasing mass loading. This is consistent with the steep increase (followed by a slow decay) of the particle outflux through the bottom once the particle-to-gas-coupling is switched on (see Figure 7). The total number of parcels in the cyclone under steady-state conditions is a clear function

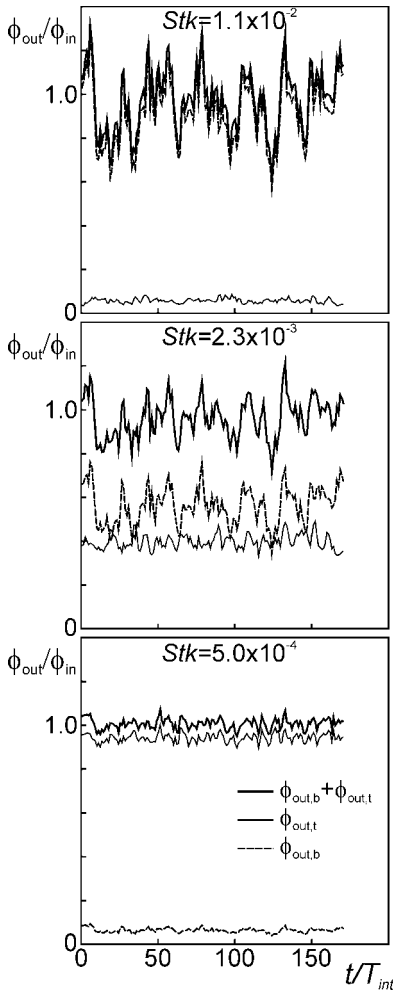

Figure 6. Quasi-steady-state time series of the particle flux through the top and bottom exhaust surfaces for three different particle sizes/Stokes numbers for a one-way couples simulation (Case 1).

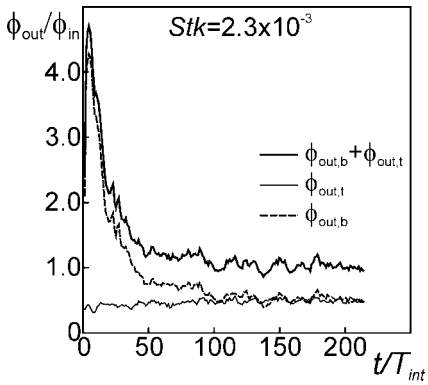

Figure 7. Time series of the particle flux through the top and bottom exhaust surfaces for $Stk = 2.3 \cdot 10^{-3}$.

At moment $t = 0$ we switch from a fully developed (in terms of gas and solids) one-way coupled simulation (Case 1) to a two-way coupled simulation with mass loading of $\phi_m = 0.025$ (Case 6).

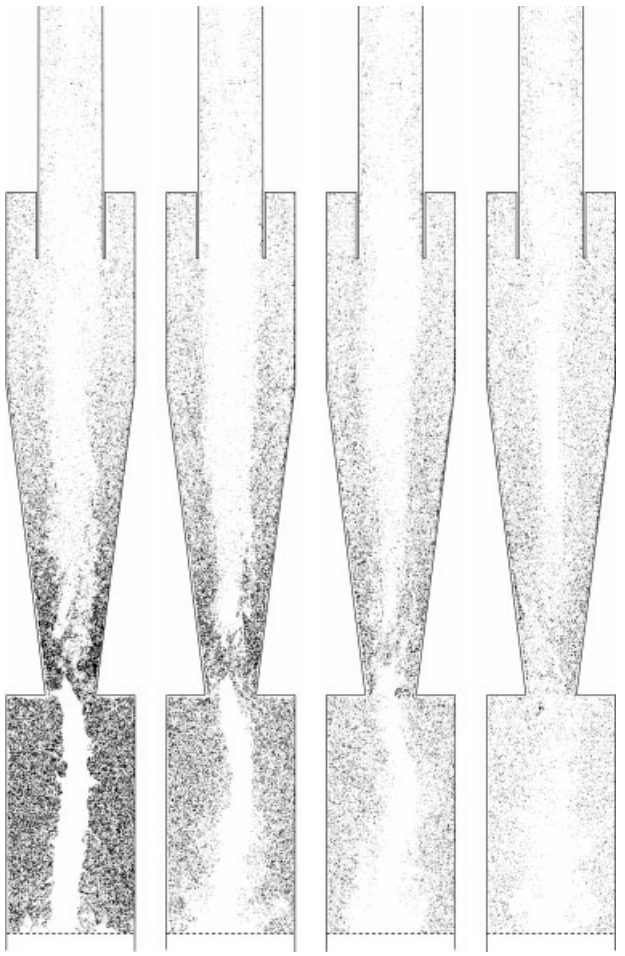

Figure 8. Instantaneous realizations of the particles with $Stk = 2.3 \cdot 10^{-3}$ in vertical slice, with thickness of 0.02*D* through the center of the cyclone (the *xy*-plane) in (from left to right) a one-way coupled simulation, and two-way coupled simulations with mass-loading 0.00625, 0.025, and 0.1, respectively.

of the solids loading (see Figure 9). The higher the loading, the less parcels are present in the cyclone. The total solids mass in the cyclone (number of parcels times γ times the mass of each particle), however, increases with the mass loading of the feed stream (see also Figure 9). An additional observation that can be made from Figure 8 is that the dispersion of the $Stk = 2.3 \cdot 10^{-3}$ particles gets stronger at higher mass loading: The part of the vortex core void of particles is definitely narrower in the higher loading cases.

Time averaged, radial solids concentration profiles for the various Stokes numbers at various axial levels in the cyclone as given in Figure 10 reflect the competition between centrifugal forces and dispersion. Smaller particles are spread throughout the cyclone; bigger particles accumulate near the walls. In the higher portion of the cyclone, the particle concentration field is relatively insensitive to the mass loading. Deeper in the cyclone the particle concentration decreases with increasing mass loading. As we will see, this effect

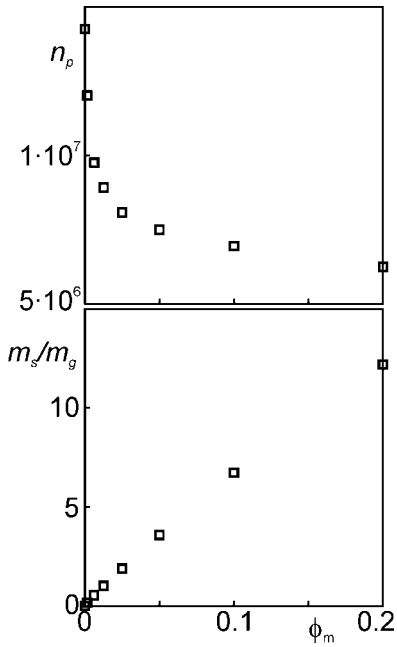

Figure 9. Total number of parcels (top), and total solids mass (normalized with the total mass of gas) inside the Stairmand cyclone under steady-state conditions as a function of the mass loading (zero mass loading: one-way coupled, $\phi_m > 0$: two-way coupled).

relates to the way the presence of the particles affects the strength of the swirl and of the turbulence.

Loading effects on the gas velocity field

Swirl reduction and turbulence damping due to particles in the Stairmand cyclone can be witnessed from Figure 11. This figure shows gas velocity data at various axial levels in the cyclone under various mass loading conditions. The trends with respect to the swirl velocity are very clear: the presence of particles systematically reduces the swirl velocity. The reduction of swirl is mostly felt in the free-vortex part of the swirl profile, since here the particle concentrations are much higher than in the core. To quantify the swirl reduction, we plot it in Figure 12 as the ratio of the maximum tangential velocity under loaded conditions over that under zero loading conditions at a specific axial location vs. the mass loading. We see that the reduction of swirl depends on the axial level: the deeper in the cyclone, the stronger the tangential velocity gets reduced: The particles attenuate the penetration of swirl into the cyclone. Swirl gets reduced by roughly 50% for a mass loading of 0.2.

In swirling flows, the axial velocity is largely slaved to the tangential velocity: the way the swirl develops axially determines the axial pressure gradient that in turn determines the velocity in axial direction. As a result, the axial velocity profiles (shown in the middle column of Figure 11) respond to the swirl reduction due to the particles. The lesser swirl makes the axial velocity profiles less pronounced and shallows (or

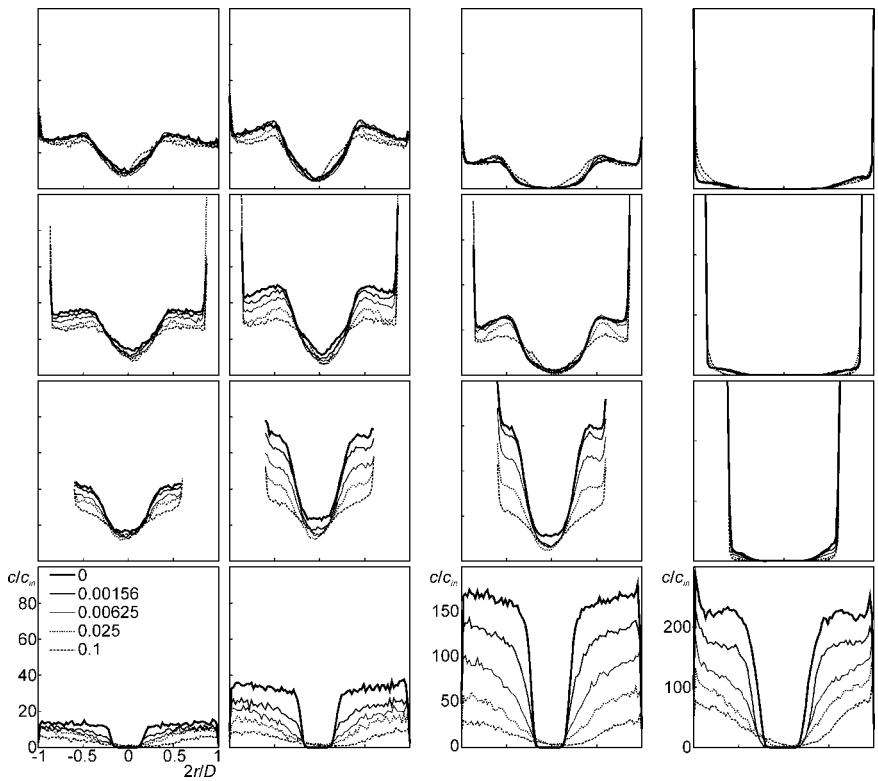

Figure 10. Radial profiles of the time averaged particle number concentration (normalized with the concentration at the inlet c_{in}).

From top to bottom the axial levels are x/D = 3.25, 2.0, 1.0, −1.0. From left to right the Stokes numbers are $Stk = 3{\cdot}10^{-4}$, $8.3{\cdot}10^{-4}$, $2.3{\cdot}10^{-3}$, $1.1{\cdot}10^{-2}$. The various curves per panel indicate mass loading ($\phi_m = 0$: one-way coupled, $\phi_m > 0$: two-way coupled).

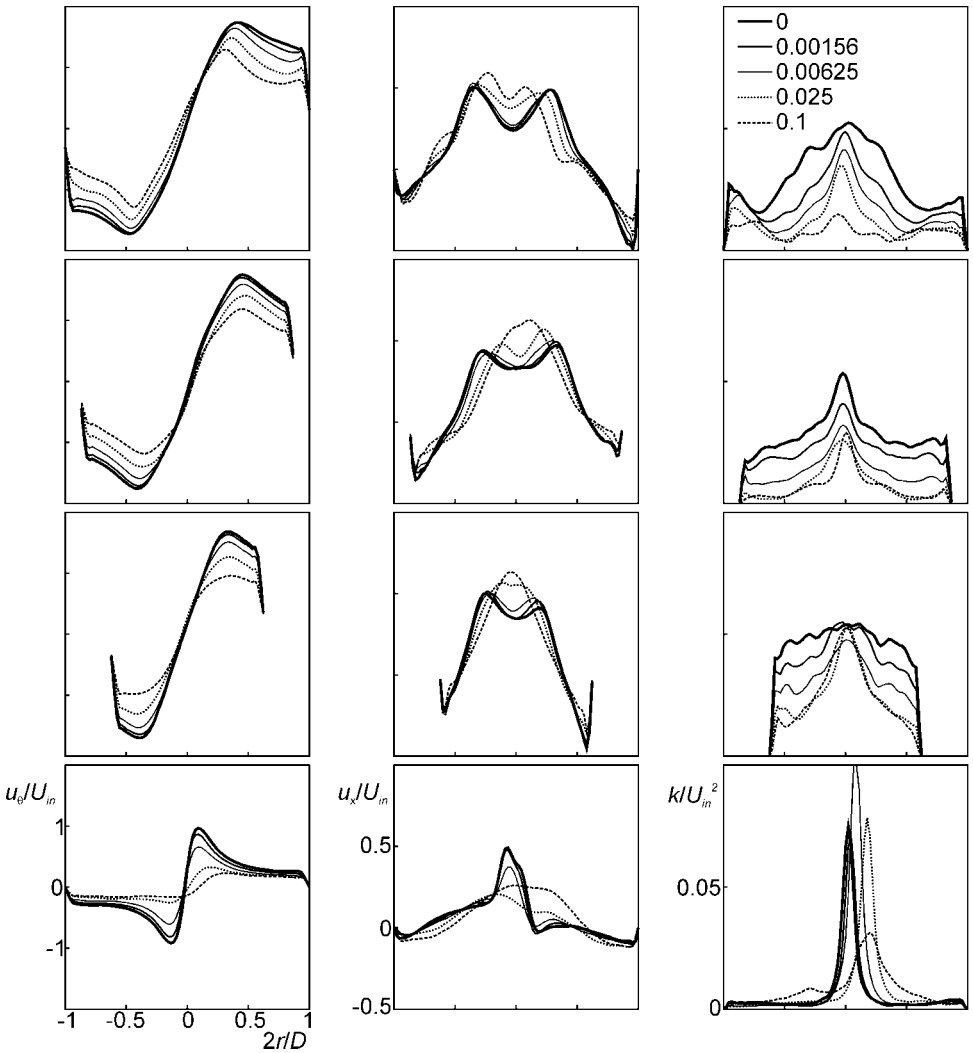

Figure 11. Radial profiles of the time averaged gas flow under various mass loading conditions (ϕ_m = 0: one-way coupled, ϕ_m > 0: two-way coupled).

From left to right: tangential velocity, axial velocity, and turbulent kinetic energy k. From top to bottom the axial levels are x/D = 3.25, 2.0, 1.0, −1.0.

even takes away) the local minimum in the axial velocity profile close to the center. The turbulent kinetic energy (k) reduction as a result of the particles shows a consistent trend as well, see the right column of Figure 11. A mass loading of ϕ_m = 0.1 in some places reduces k by one order of magnitude. The effects are not as systematic as they are for the swirl velocity. For some cases and axial positions swirl is specifically reduced in the center, for others in the free vortex region. In the dustbin the turbulent kinetic energy responds rather erratically to the mass loading. This has no significant effect on the particle behavior since the effects are confined to a relatively narrow region close to the center of the dustbin where not many particles are present. In the outer zones of the dustbin gas velocity fluctuations are very small.

Cyclone performance has two major aspects: pressure drop and separation efficiency. From the gas phase velocity results we can anticipate a pressure drop reduction as a result of mass loading since lower swirl velocities imply lower wall

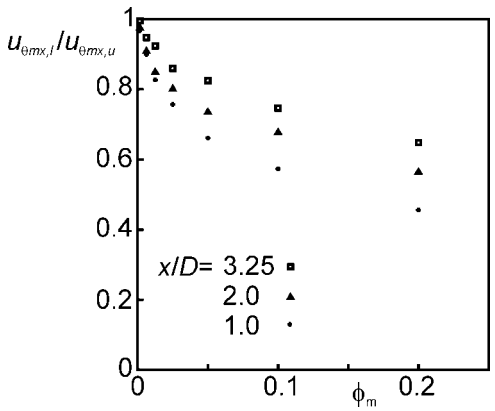

Figure 12. Decay of the swirl velocity in terms of the ratio of the maximum swirl velocity under loaded ($u_{\theta mx,l}$) and unloaded ($u_{\theta mx,u}$) conditions as a function of mass loading for three axial levels in the cyclone.

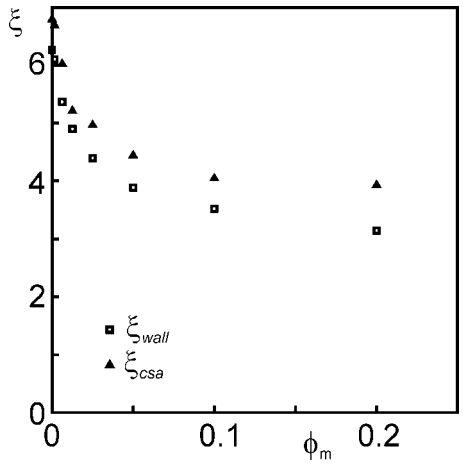

Figure 13. Pressure drop coefficient as a function of the mass loading.

We distinguish between cross-sectional-averaged (*csa*) pressure drop, and pressure drop determined at the wall.

friction, and, thus, reduced pressure drop. As discussed earlier, it is *a priori* not clear what the net effect of swirl reduction and turbulence reduction on the separation efficiency will be.

Cyclone performance: pressure drop and collection efficiency

Swirling flows have a pronounced radial pressure profile. This requires caution when defining pressure drop. In this study pressure drop is defined as it is usually done when performing pressure measurements at walls: We define the pressure drop as the pressure at the inner wall of the vortex finder (at $x = 4.5D$) minus the pressure at the wall in the inlet channel. In the inlet channel the pressure is more or less uniform. The pressure at the wall in the vortex finder fluctuates as a result of turbulence, so that a sufficiently long averaging time is required. For this we take at least $50T_{int}$.

The time-averaged pressure drop coefficient $\xi_{wall} = \frac{\Delta p}{\frac{1}{2}\rho_g U_{in}^2}$ as a function of mass loading is given in Figure 13. This graph shows qualitative agreement with results reported from experiments by Hoffmann et al.[8] They also used (variants of) Stairmand cyclones. The geometry they denoted by II has the same dimensions as the cyclone we investigate, except for the dustbin that is absent in their work. The highest Reynolds number they reached was $Re = 8{\cdot}10^4$ (with an inlet velocity of 20 m/s), which is roughly a factor of 3 below our Reynolds number. As a result, some caution is required in comparing their and our results in a quantitative manner. Their pressure drop coefficient at zero loading is 5.6, our LES has 6.1. At their maximum loading ($\phi_m = 0.03$), the pressure drop coefficient has reduced to 4.2. Interpolating in Figure 13 to $\phi_m = 0.03$, and taking the results for ξ_{wall} we get a value of 4.4. This is good agreement, specifically in light of the differences between the experimental and numerical work.

It is interesting to also check the pressure drop in terms of the pressure averaged over the cross sectional area in the vortex finder (again at $x = 4.5D$), since this is the pressure drop relevant for the power consumed by the cyclone. These data (indicated as ξ_{csa} in Figure 13) show the same trend, with a slightly weaker dependency on the mass loading. This is because the swirl intensity in the vortex finder (and, thus, the radial pressure profile) gets weaker for higher mass loadings.

Finally, we present results with respect to the collection efficiency as a function of mass loading. As discussed earlier, measuring collection efficiency requires a quasi steady gas and particle flow field. A good way to check this is to determine the collection efficiency per particle size/Stokes number in two ways: The first is related to fluxes through the bottom: it is the time-averaged particle flux through the bottom normalized by the influx, as a function of *Stk*: $\eta_{bottom} = \frac{\phi_{out,bottom}(Stk)}{\phi_{in}}$. The second is based on the exhaust of particles through the top: $\eta_{top} = 1 - \frac{\phi_{out,top}(Stk)}{\phi_{in}}$. The two curves should overlap under steady-state conditions, and with long enough averaging times. As an example, we show the two curves along with the average of both in Figure 14 for the two-way coupled simulation with $\phi_m = 0.0125$. Their (small) deviation is a good measure for the error margins due to statistical effects. In what follows, grade efficiencies are the average of η_{top} and η_{bottom}.

Grade efficiency curves at various mass loadings are given in Figure 15. The trends with respect to mass loading are quite subtle. For small loadings the cut size slightly decreases, followed by a significant increase for higher mass loadings. Small particles get better collected when the mass loading is small; collection of bigger particles improves with higher mass loading. These effects are further detailed in Figure 16. The overall collection efficiency, defined as $\eta_{overall} = \int_0^1 \eta(d_p)d\Phi$ (with η the grade efficiency, and Φ the cumulative volume density distribution of the powder) very sharply increases with mass loading under low ($\phi_m < 0.01$) loading conditions. At higher loadings it decreases again, but is still appreciably higher than the efficiency under zero loading (~93.5% vs ~91%).

It should be noted, however, that since the efficiency depends on mass loading, and since particles with different sizes get dispersed differently in the cyclone, the shape of the particle-size distribution itself contributes to the extent of

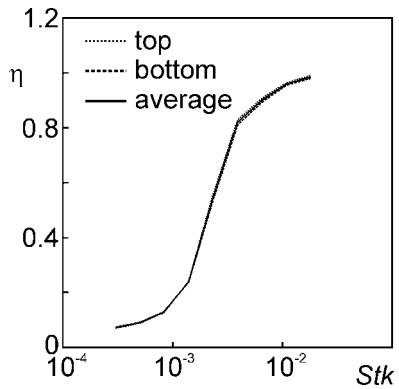

Figure 14. Grade efficiency for the two-way coupled simulation with $\phi_m = 0.0125$ (Case 5) as measured through the top, the bottom and the average of these two.

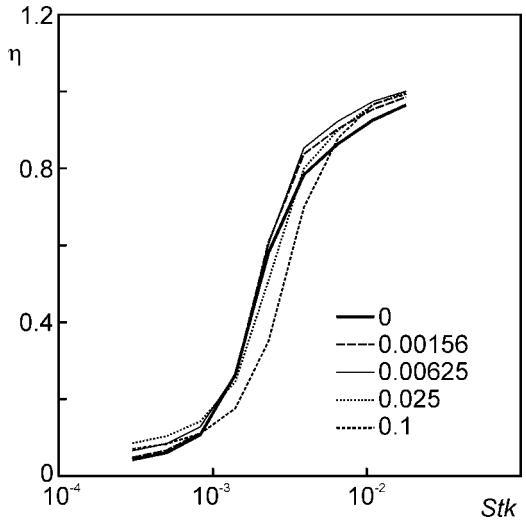

Figure 15. Grade efficiency curves for various mass loadings ($\phi_m = 0$: one-way coupled, $\phi_m > 0$: two-way coupled).

the mass loading effect. To not further broaden the parameter space in this article, we have only investigated situations with a uniform particle-size distribution at the inlet of the cyclone.

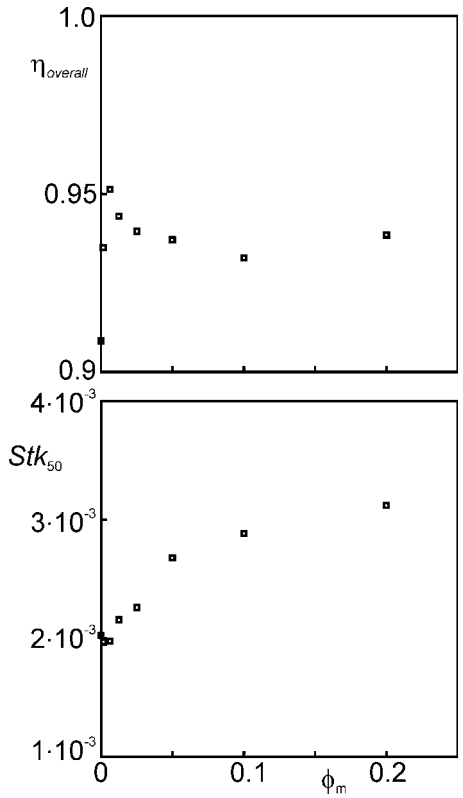

Figure 16. Stk_{50} (the Stokes number for which 50% of the particles is collected) as a function of mass loading (bottom), and the overall efficiency as a function of mass loading (top).

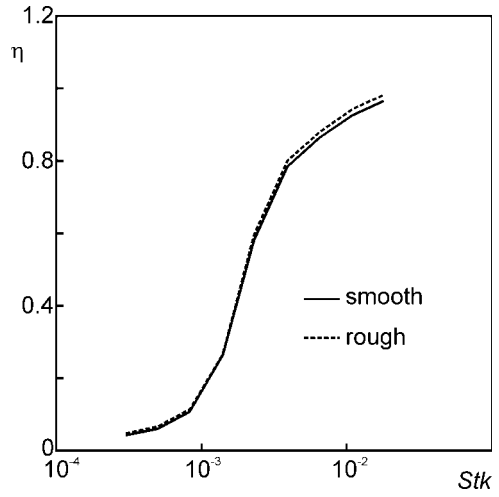

Figure 17. Grade efficiency, effect of particle boundary conditions. Comparison of the one-way coupled simulations 1 and 2.

"Smooth" indicates specular reflection with restitution coefficient 1.0, rough means diffuse reflection with restitution coefficient 0.9.

So far the particle-wall collisions were fully elastic and frictionless, i.e., particles get specularly reflected and do not loose energy during the collision. In order to check how sensitive the results for the separation efficiency are with respect to this assumption, a one-way coupled simulation was setup with rough walls in which the particles reflected diffusively (i.e., the direction of the velocity with which particles bounce off the wall back into the cyclone is random according to uniform angle distributions). Furthermore the restitution coefficient was set to 0.9. This simulation (Case 2, see Table 1

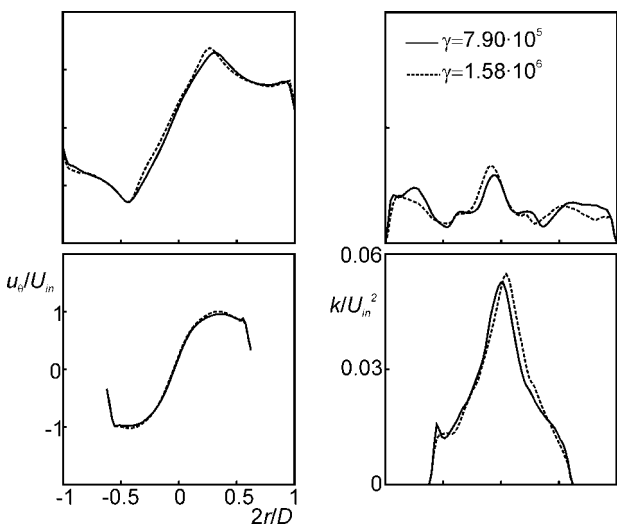

Figure 18. Swirl and turbulent kinetic energy profiles at $x/D = 3.25$ (top), and 1.0. Sensitivity with respect to the number of particles per parcel γ. Two-way coupled simulations with $\phi_m = 0.1$ (cases 8 and 9).

was started from a fully developed one-way coupled gas-solid field with smooth walls. Interestingly, the time series of the particle outfluxes initially respond slightly to this change in particle boundary conditions. However, once the gas-solid system gets back to a steady state, only small differences in terms of the grade efficiency as compared to the default particle-wall collisions can be observed (see Figure 17); with a slightly higher collection efficiency in the rough-wall situation for the bigger particles. The latter trend is perfectly understandable: particles colliding with a rough wall on average stay closer to the wall, and, therefore, have a lesser chance to get dispersed by turbulence.

Another check relates to the number of particles per parcel. The case with $\phi_m = 0.1$ (Case 8) was compared with a case with half the number flux of parcels at the inlet and twice as many particles per parcel (Case 9), i.e., the same loading condition under different numerical parameters. In Figure 18 we show swirl velocity profiles and kinetic energy profiles of the two cases. No remarkable differences are observed.

Conclusions

In this article, the effect of mass-loading on the gas flow and solid particle motion in a Stairmand high-efficiency cyclone separator has been studied numerically. Our Eulerian-Lagrangian simulations confirm that the separation process involves an interplay between centrifugal forces induced by swirl, and dispersion due to turbulence. We qualitatively validated the way we account for the effect of the particles on the gas stream by simulating two-phase cyclone cases experimentally studied by Obermair et al.[17] The trends they observed with respect to the gas-swirl field were reproduced by our simulations: a reduction of the tangential velocity and widening of its profile. The single and two-phase flow cases due to Obermair et al.[17,18] again demonstrated the need for fine grids to accurately capture the details of the gas-flow field in terms of its average velocity and fluctuation levels. For simulating appreciable mass loadings, the number of particles per parcel γ has to be of the order of $10^4 - 10^6$. We showed for the case of mass loading 0.1 that the LES results for the gas-flow field are quite insensitive to the choice of the numerical parameter γ.

Another key feature of this work has been the length of the simulations as measured in the number of integral time scales needed to reach steady state of the gas-solid flow fields, and, subsequently, to reach statistically converged grade efficiencies. The fluctuations of the fluxes of the bigger particles leaving the cyclone have large time scales (of the order of 30 integral time scales). This required the simulation of the quasi-steady state two-phase flow for some 150 integral time scales. A typical simulation ran in parallel on 12 nodes of a PC cluster for a number of weeks.

In our calculations, both swirl and turbulence are affected by the presence of particles, even at the relatively modest solids loadings that we have considered. The swirl in the cyclone monotonically reduces with increasing mass loading of particles. This effect is strongest in the lower parts of the cyclone: the particles obstruct the penetration of swirl in the cyclone. At a mass loading of 0.2, swirl reduces by some 50%. The turbulent fluctuations also strongly reduce with increasing mass loading of particles. This occurs in a more complicated way than the swirl reduction. At some locations, turbulent kinetic energy reduces by an order of magnitude. At other locations (especially near the center) there is hardly any reduction of turbulence intensity. The dustbin shows sharply peaked turbulent kinetic energy profiles irrespective of mass loading.

Since the tangential velocity component is the largest it largely determines the boundary layer at the cyclone's outer wall. Swirl reduction, therefore, implies less wall friction. As a result, the pressure drop over the cyclone gets lower with increased mass loading. The extent of this effect is in good agreement with what has been measured by e.g., Hofmann et al.[8]

As both turbulence attenuation and weakening of the swirl occur with increased mass loading of particles, one can readily envision the possibility of complex dependence of collection efficiency on particle mass loading. Turbulence attenuation can be expected to improve efficiency while a weakening of the swirl intensity will have the opposite effect. Thus, depending on the relative extents of turbulence attenuation and weakening of swirl intensity, the efficiency of the cyclone can either increase or decrease. For very low-mass loadings (<0.01) we see a very slight reduction of the cut size (the value of Stk_{50} reduces by a few percent). Here the swirl reduction is minimal, whereas turbulence (especially in the free vortex region) is already strongly reduced. At higher loadings, Stk_{50} increases strongly (with 50% at $\phi_m = 0.2$). Our simulations have demonstrated unequivocally that mass loading influences collection efficiency through its effect on both swirl and turbulence intensities. Complex variation of the collection efficiency with mass loading, whenever observed in experiments, can now be rationalized through an interplay of these two effects.

Compared to the one-way coupled (i.e., $\phi_m = 0$) simulation, all two way coupled simulations have higher overall efficiencies (particle mass collected over particle mass inserted). This is largely due to the fact that the bigger particles get better collected. We note that the shape of the particle-size distribution fed to the cyclone will have impact on the cyclone's collection efficiency. The way particles get dispersed in the cyclone depends on their size. The dispersion affects the particle-to-gas coupling which affects the efficiency. In this article, we did not consider the influence of the shape of the particle-size distribution on the cyclone performance; we only fed the cyclone with a uniform size distribution.

Wall boundary conditions for the particles did not have big impact on the separation process. We compared a smooth wall with a rough wall and found only marginally better collection of coarse particles with a rough walled cyclone.

Acknowledgment

The authors wish to thank Dr. Günter Gronald (TU Graz) for making available experimental data, and for helpful discussions.

Literature Cited

1. Gupta AK, Lilley DG, Syred N. *Swirl flows*. Tunbridge Wells, UK: Abacus Press; 1984.

2. Escudier M. Vortex breakdown, observations and explanations. *Progress Aerospace Sc*. 1988;25:189–229.
3. Wunenburger R, Andreotti B, Petitjeans P. Influence of precession on velocity measurements in a strong laboratory vortex. *Experiments in Fluids*. 1999;27:181–188.
4. Derksen JJ. Simulations of confined turbulent vortex flow. *Computers & Fluids*. 2005;34:301–318.
5. Muschelknautz E. Theorie der fliehkraftabscheider mit besonderer berücksichtigung hoher temperaturen und drücke. *VDI Berichte*. 1980;363:49–60.
6. Mothes H, Löffler F. Motion and deposition of particles in cyclones. *Chem Ingenieur Technik*. 1984;56:714–715.
7. Derksen JJ. Separation performance predictions of a Sairmand high-efficiency cyclone. *AIChE J*. 2003;49:1359–1371.
8. Hoffmann AC, Arends H, Sie H. An experimental investigation elucidating the nature of the effect of solids loading on cyclone performance. *Filt & Sep*. 1991;28:188–193.
9. Hoffmann AC, Van Santen A, Allen RWK. Effects of geometry and solid loading on performance of gas cyclones. *Powder Technol*. 1992;70:83–91.
10. Muschelknautz E. Die berechnung von zyklonabscheidern für gase. *Chem Ingenieur Technik*. 1972;44:63–71.
11. Derksen JJ, Sundaresan S, Van den Akker HEA. Simulation of mass-loading effects in gas-solid cyclone seprators. *Powder Technol*. 2006;163:59–68.
12. Yuu S, Jotaka T, Tomita Y, Yoshida K. The reduction of pressure drop due to dust loading in a conventional cyclone. *Chem Eng Sc*. 1978;33:1573–1580.
13. Muschelknautz E, Brunner K. Experiments with cyclones. *Chem Ingenieur Technik*. 1967;39:531–538.
14. Gore RA, Crow CT. Effect of particle size on modulating turbulent intensity. *I J Multiphase Flow*. 1989;15:279–285.
15. Fessler JR, Eaton JK. Turbulence modification by particles in a backward-facing step flow. *J Fluid Mech*. 1999;394:97–117.
16. Derksen JJ, Van den Akker HEA. Simulation of vortex core precession in a reverse-flow cyclone. *AIChE J*. 2000;46:1317–1331.
17. Obermair S, Gutschi C, Woisetschläger J, Staudinger G. Flow pattern and agglomeration in the dust outlet of a gas cyclone investigated by phase doppler anemometry. *Powder Technol*. 2005;156,34–42.
18. Obermair S, Woisetschläger J, Staudinger G. Investigation of the flow pattern in different dust outlet geometries of a gas cyclone by laser doppler anemometry. *Powder Technol*. 2003;138:239–251.
19. Chen S, Doolen GD. Lattice boltzmann method for fluid flows. *Annual Rev Fluid Mech*. 1998;30:329–364.
20. Succi S. The lattice Boltzmann equation for fluid dynamics and beyond. Oxford: Clarondon Press; 2001.
21. Goldstein D, Handler R, Sirovich L. Modeling a no-slip flow boundary with an external force field. *J Comp Phys*. 1993;105:354–366.
22. Derksen JJ, Van den Akker HEA. Large eddy simulations on the flow driven by a Rushton turbine. *AIChE J*. 1999;45:209–221.
23. Verzicco R, Mohod-Yusof J, Orlandi P, Haworth D. Large-eddy-simulation in complex geometric configurations using boundary body forces. *AIAA J*. 2000;38:427–433.
24. Smagorinsky J. General circulation experiments with the primitive equations: part I, the basic experiment. *Monthly Weather Rev*. 1963;91:99–164.
25. Escudier MP, Bornstein J, Maxworthy T. The dynamics of confined vortices. *Proc Royal Soc London A*. 1982;382:335–360.
26. Benjamin TB. Theory of the vortex breakdown phenomenon. *J Fluid Mech*. 1962;14:593–629.
27. Hoekstra AJ, Gas flow field and collection efficiency of cyclone separators. Delft University of Technology, Netherlands; 2000. PhD Thesis.
28. Schiller L, Naumann A. Uber die grundlagenden berechnungen bei der schwerkraftaufbereitung. *Ver Deut Ing Z*. 1933;77:318–320.
29. Mason PJ, Callen NS. On the magnitude of the subgrid-scale eddy coefficient in large-eddy simulations of turbulent channel flow. *J Fluid Mech*. 1986;162:439–462.
30. Crowe CT, Troutt TR, Chung JN. Numerical models for two-phase turbulent flows. *Annual Rev Fluid Mech*. 1996;28:11–42.
31. Gronald G. Private communications; 2005.

Manuscript received July 25, 2007, and revision received Nov. 3, 2007.